Journal of High Energy Astrophysics 26 (2020) 11–20

Contents lists available at ScienceDirect

Journal of High Energy Astrophysics

www.elsevier.com/locate/jheap

# A modified direct demodulation method applied to *Insight-HXMT* Galactic plane scanning survey

Ju Guan [a,*], Fang-Jun Lu [a], Shu Zhang [a], Li-Ming Song [a], Yong Chen [a], Jin-Yuan Liao [a], Cheng-Kui Li [a], Yi Nang [a,b], Na Sai [a,b], Chen Wang [b,c], Shuang-Nan Zhang [a,b,c]

[a] *Key Laboratory of Particle Astrophysics, Institute of High Energy Physics, Chinese Academy of Sciences, Beijing 100049, China*
[b] *University of Chinese Academy of Sciences, Beijing 100049, China*
[c] *Key Laboratory of Space Astronomy and Technology, National Astronomical Observatories, Chinese Academy of Sciences, Beijing 100012, China*

ARTICLE INFO

*Article history:*
Received 12 December 2019
Received in revised form 10 February 2020
Accepted 17 February 2020

*Keywords:*
Methods: data analysis
X-rays: variable sources
Telescope: Insight-HXMT

ABSTRACT

We present a modified direct demodulation (DD) method for the detection of fast variable objects with the *Insight-HXMT* Galactic plane survey, which is dedicated to hunting for new transients and monitoring known variable sources. The novelty of the improved DD method is the reconstruction of the modified response matrix, in which the variability of a source is properly handled. Monte Carlo (MC) simulation results demonstrate its power for the detection of variable sources with different time scales, resulting in more accurate location and precise flux monitoring. The application of the method to the *Insight-HXMT* Galactic plane survey data reveals that the type-II bursts can be well detected for the Rapid Burster MXB 1730–335, with an average rate of 2 bursts $min^{-1}$ in a manner of the well-known relaxation oscillation.


## 1. Introduction

The newly launched Hard X-ray Modulation Telescope (dubbed as *Insight-HXMT*) is China's first X-ray astronomical satellite. It is designed to observe the temporal and spectral properties of bright sources in a pointing mode, and survey the Galactic plane to find new transients and to monitor known variable sources in a scanning mode, as well as hunting for gamma-ray bursts (GRBs) in a GRB mode (Zhang et al., 2019). It has three slat-collimated payloads on board: the High Energy Telescope (HE, $20-250$ keV, 5100 $cm^2$), the Medium Energy Telescope (ME, $5-30$ keV, 952 $cm^2$), and the Low Energy Telescope (LE, $1-15$ keV, 384 $cm^2$) (Liu et al., 2019; Cao et al., 2019; Chen et al., 2019). For each payload the Point Spread Function (PSF) and field of view (FoV) are confined by the collimators. Thus a source can leave its footprint in the light curve with a triangle shaped peak once it is scanned. During the *Insight-HXMT* Galactic plane survey, the three payloads work in a similar way: the source count rate will be sampled by the PSF and the source photons will be recorded by the non-position-sensitive detectors. Using the recorded data from survey and the instrumental PSF, sky image can be reconstructed with a proper inversion method and hence the source properties such as flux and location, can be derived accordingly.

There exist many methods to obtain the source properties such as fluxes and locations in high energy astronomy (Starck and Murtagh, 2006), e.g., cross correlation is proved to be the simplest and most convenient linear method for detecting point sources and is widely used in the COS-B and EXOSAT data analysis; the statistical methods such as the maximum entropy method (Gull and Daniell, 1978) provide statistical solutions to the reconstruction process. In addition to these techniques, an innovative inversion method—Direct Demodulation (DD) method (Li and Wu, 1993, 1994), was proposed. It usually consists of two steps. First the background is derived by iteratively solving the modulation equation or the correlation equation under continuous constraints. Then, the intensity distribution of the object sky is obtained by solving the equation again under constraints of the produced background as a lower limit. After subtracting the background, the true intensity distribution of the sources can be derived. As each iterative calculation is directly based on the modulation equation, the DD method could use all the information in the modulation equation. While introducing physical constraints to put nonlinear control on each iteration, the iterative process is stable and convergent. Any kind of a *priori* knowledge can be also easily included in the modulation equation or the constraints, making DD method a flexible technique. The convergency and global optimization of DD method has been proven

* Corresponding author.
*E-mail address:* jguan@ihep.ac.cn (J. Guan).

https://doi.org/10.1016/j.jheap.2020.02.002
2214-4048/

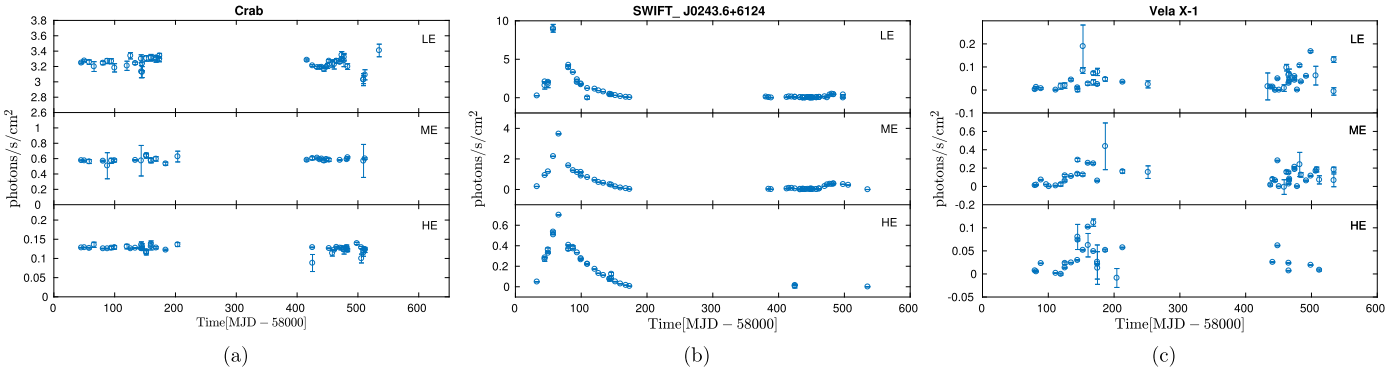


**Fig. 1.** Long-term light curves of the Crab nebula (a), Swift J0243.6+6124 (b) and Vela X–1 (c) obtained with the *Insight-HXMT* Galactic plane survey (http://hxmt.org/index.php/usersp/dataan/sourcelist).

by the theory of neural computing (Li, 2003). Bootstrap technique is usually applied to estimate the statistic uncertainties of the source restored in the sky image (Li and Wu, 1993). DD method has been successfully applied to the analysis of the data from a variety of telescopes, e.g., slat collimator telescope (EXOSAT/ME (Lu et al., 1996), HEAO1-A4 (Lu et al., 1995), RXTE/ASM (Song et al., 1999)), coded aperture mask telescope (INTEGRAL/ISGRI (Shen and Zhou, 2008)), imaging telescope (COS-B (Li and Wu, 1993), ROSAT/PSPC (Chen et al., 1997), XMM-Newton (Feng et al., 2003)), and Compton scattering telescope (CGRO/COMPTEL (Zhang et al., 1998)). The good quality of the reconstructed images demonstrates that DD method could reach higher resolution and is flexible to reconstruct the image of complicated regions even from incomplete and noisy data. The DD method is thus a main image reconstruction technique to analyze the scan observation data of *Insight-HXMT*. After 2-year Galactic plane survey, some scientific products have been obtained with this method: high resolution X-ray sky map, X-ray point source catalogue with more than 800 sources and their long-term light curves (Fig. 1), a map of the Galactic diffuse emission etc., which will be reported in later papers and some of them were shown in Zhang et al. (2019).

However, so far the DD method is developed under an assumption that source flux is stable. This hypothesis stands in most cases if long-term variability can be treated as a series of short-term invariables. For example, the outbursts of many X-ray binaries last for weeks or even months. However, compared to the time scale of $\sim 3$ hours for an individual scanning observation of one patch of the Galactic plane with *Insight-HXMT*, these sources in most cases can be regarded approximately stable in the 3 hours and thus the DD method can be adopted to derive the flux of the sources. Indeed the light curves of sources at time scale of hours are the expected routine product of the *Insight-HXMT* Galactic plane survey. However, the Galactic plane is a big zoo with sources of different time variabilities. Among them, an interesting class of sources called Supergiant Fast X-ray Transients (SFXT) show very quick transient nature, with bright X-ray flares of short duration (from a few minutes to a few hours) (Paizis and Sidoli, 2014). A more extreme transient example is the Type-II Bursts which could be as short as 0.130 s (Bagnoli et al., 2015). In reality there does exist in *Insight-HXMT* Galactic plane survey data fast variable events like fast short bursts which have typical duration of ∼10 s and waiting time of a few tens of seconds or longer. In such cases the sources can no longer be treated as invariable and in order to restore the flux of these sources properly one needs an improved DD method. Hence, a modified DD method is proposed to address this problem. Another issue addressed in the improved DD method is about how to handle the background. The previous DD method reconstructs firstly the background data and then uses the result as the lower limit in restoring the sky image from the observational data. In the improved DD method, the background model derived directly from the observational data is properly included in a new iteration equation.

The paper is organized as follows. In section 2, we give a brief description of the improved DD method based on the new iteration equation and some other techniques. The results obtained with this improved DD method, to both the MC data and real *Insight-HXMT* data, are presented in section 3. Discussions and conclusions are carried out in section 4.

## 2. Method

### 2.1. The modulation equation and the modified modulation equation

For a telescope, an observation of an object can be regarded as a modulation process of signal from object via detection by the instrument, which could be described by the modulation equation:

$$D = PF + B, \tag{1}$$

where $F$ and $D$ represent the intensity distributions of a sky region in the object space and the data recorded by the instrument in the data space, respectively, while $P$ and $B$ denote the response matrix and the background. For an object space with $N$ pixels and a data space with $M$ bins, Eq. (1) in discretization form constitutes an algebraic equation:

$$d(k) = \sum_{i=1}^{N} P(k,i) f(i) + b(k), \qquad (k = 1, 2, ..., M) \tag{2}$$

or

$$\begin{bmatrix} d_1 \\ d_2 \\ \vdots \\ d_M \end{bmatrix} = \begin{bmatrix} P_{11} & P_{12} & \cdots & P_{1N} \\ P_{21} & P_{22} & \cdots & P_{2N} \\ \vdots & \vdots & \ddots & \vdots \\ P_{M1} & P_{M2} & \cdots & P_{MN} \end{bmatrix} \begin{bmatrix} f_1 \\ f_2 \\ \vdots \\ f_N \end{bmatrix} + \begin{bmatrix} b_1 \\ b_2 \\ \vdots \\ b_M \end{bmatrix}$$
$$= \begin{bmatrix} P_{11} \\ P_{21} \\ \vdots \\ P_{M1} \end{bmatrix} f_1 + \begin{bmatrix} P_{12} \\ P_{22} \\ \vdots \\ P_{M2} \end{bmatrix} f_2 + \cdots + \begin{bmatrix} P_{1N} \\ P_{2N} \\ \vdots \\ P_{MN} \end{bmatrix} f_N$$
$$+ \begin{bmatrix} b_1 \\ b_2 \\ \vdots \\ b_M \end{bmatrix}, \tag{3}$$

which indicates that the observational data are the sum of a series of convolutions of the instrument response with the individual pixels in the object space. For an observational mode of scanning, the data space is constituted by a time sequence of light curve and, along with time elapse of the scanning, each bin represents the contribution of all pixels at a given time. Thus, if a source undergoes a burst, the response of this source can be treated as a combination of quiescence and bursts. Since the burst will give contribution only to those bins covered by the burst duration, only the bins corresponding to the bursting time sequence in the response matrix remain and the others should be replaced with zero. The mathematical representative of such an idea is:

$$
\begin{aligned}
D &= \begin{bmatrix} d_1 \\ d_2 \\ d_3 \\ d_4 \\ d_5 \\ d_6 \\ d_7 \\ d_8 \\ d_9 \\ \vdots \\ d_M \end{bmatrix} = \begin{bmatrix} P_{11} \\ P_{21} \\ P_{31} \\ P_{41} \\ P_{51} \\ P_{61} \\ P_{71} \\ P_{81} \\ P_{91} \\ \vdots \\ P_{M1} \end{bmatrix} f_1^{\text{quiescence}} + \begin{bmatrix} 0 \\ P_{21} \\ P_{31} \\ 0 \\ 0 \\ 0 \\ 0 \\ 0 \\ 0 \\ \vdots \\ 0 \end{bmatrix} f_1^{\text{burst1}} \\
&+ \begin{bmatrix} 0 \\ 0 \\ 0 \\ 0 \\ P_{51} \\ 0 \\ 0 \\ 0 \\ 0 \\ \vdots \\ 0 \end{bmatrix} f_1^{\text{burst2}} + \cdots + \begin{bmatrix} 0 \\ 0 \\ 0 \\ 0 \\ 0 \\ 0 \\ 0 \\ P_{81} \\ P_{91} \\ \vdots \\ 0 \end{bmatrix} f_1^{\text{burst}L} \\
&+ \begin{bmatrix} P_{12} \\ P_{22} \\ P_{32} \\ P_{42} \\ P_{52} \\ P_{62} \\ P_{72} \\ P_{82} \\ P_{92} \\ \vdots \\ P_{M2} \end{bmatrix} f_2 + \cdots + \begin{bmatrix} P_{1N} \\ P_{2N} \\ P_{3N} \\ P_{4N} \\ P_{5N} \\ P_{6N} \\ P_{7N} \\ P_{8N} \\ P_{9N} \\ \vdots \\ P_{MN} \end{bmatrix} f_N + \begin{bmatrix} b_1 \\ b_2 \\ b_3 \\ b_4 \\ b_5 \\ b_6 \\ b_7 \\ b_8 \\ b_9 \\ \vdots \\ b_M \end{bmatrix} \\
&= \begin{bmatrix} P_{11} & P_{12} & \cdots & P_{1N} & 0 & 0 & \cdots & 0 \\ P_{21} & P_{22} & \cdots & P_{2N} & P_{21} & 0 & \cdots & 0 \\ P_{31} & P_{32} & \cdots & P_{3N} & P_{31} & 0 & \cdots & 0 \\ P_{41} & P_{42} & \cdots & P_{4N} & 0 & 0 & \cdots & 0 \\ P_{51} & P_{52} & \cdots & P_{5N} & 0 & P_{51} & \cdots & 0 \\ P_{61} & P_{62} & \cdots & P_{6N} & 0 & 0 & \cdots & 0 \\ P_{71} & P_{72} & \cdots & P_{7N} & 0 & 0 & \cdots & 0 \\ P_{81} & P_{82} & \cdots & P_{8N} & 0 & 0 & \cdots & P_{81} \\ P_{91} & P_{92} & \cdots & P_{9N} & 0 & 0 & \cdots & P_{91} \\ \vdots & \vdots & \ddots & \vdots & \vdots & \vdots & \ddots & \vdots \\ P_{M1} & P_{M2} & \cdots & P_{MN} & 0 & 0 & \cdots & 0 \end{bmatrix} \\
&\times \begin{bmatrix} f_1^{\text{quiescence}} \\ f_2 \\ \vdots \\ f_N \\ f_1^{\text{burst1}} \\ f_1^{\text{burst2}} \\ \vdots \\ f_1^{\text{burst}L} \end{bmatrix} + \begin{bmatrix} b_1 \\ b_2 \\ b_3 \\ b_4 \\ b_5 \\ b_6 \\ b_7 \\ b_8 \\ b_9 \\ \vdots \\ b_M \end{bmatrix} \\
&= Q\,G + B, \qquad (4)
\end{aligned}
$$

or

$$
d(k) = \sum_{i=1}^{N+L} Q\,(k,i)g(i) + b(k). \qquad (5)
$$

Here we take source $f_1$ for example. It shows up with $L$ burst events embedded in persistent evolution, with each burst known occurring time and duration. In fact, Eq. (4) works also for burst with variable flux. In this case, the flux of a burst is treated as several invariant parts and $f_1^{\text{burst}j}$ in Eq. (4) no longer represents an individual burst but an invariant part of a burst. Compared with Eq. (2), Eq. (5) allows the flux of source to change with time, we call it the modified modulation equation and $Q$ the modified response matrix.

### 2.2. Iterative solution of the modified modulation equation—a modified Richardson-Lucy (RL) equation

The modulation equation relates the observed data to the object, therefore reconstructing the object from the observed data is equivalent to solving the modulation equation. The right side of Eq. (2) and/or Eq. (5) characterizes the statistically expected value of the observed data while the observed data itself is a random outcome of the expected value for a given specific observation. For Poisson noise dominated data, the probability distribution of the observed data $D$ given the object $G$, known as likelihood (Starck and Murtagh, 2006), is:

$$
\begin{aligned}
&p(D/G) \\
&= \prod_k \frac{(\sum_{i=1}^{N+L} Q\,(k,i)g(i) + b(k))^{d(k)} \cdot e^{-(\sum_{i=1}^{N+L} Q\,(k,i)g(i)+b(k))}}{d(k)!}.
\end{aligned} \qquad (6)
$$

Maximizing the density $p(D/G)$ over $f$ gives the maximum likelihood solution of the modulation equation. Therefore the object reconstruction problem is transformed into computing the derivative of the logarithm:

$$
\frac{\partial \ln p(D/G)}{\partial g(i)} = 0, \qquad \forall i \qquad (7)
$$

leading to

$$
\begin{aligned}
&\sum_k (d(k) \frac{\partial \ln (\sum_{j=1}^{N+L} Q\,(k,j)g(j) + b(k))}{\partial g(i)} \\
&\quad - \frac{\partial (\sum_{j=1}^{N+L} Q\,(k,j)g(j) + b(k))}{\partial g(i)}) = 0, \\
&\sum_k \frac{Q\,(k,i)d(k)}{\sum_{j=1}^{N+L} Q\,(k,j)g(j) + b(k)} = \sum_k Q\,(k,i),
\end{aligned}
$$

$$\sum_k \frac{Q(k,i)d(k)}{\sum_{j=1}^{N+L} Q(k,j)g(j)+b(k)} / \sum_k Q(k,i) = 1.$$

Multiplying both sides by $g(i)$ and using Picard iteration leads to

$$g^{(r+1)}(i) = g^{(r)}(i) \sum_k \frac{Q(k,i)d(k)}{\sum_{j=1}^{N+L} Q(k,j)g(j)+b(k)} / \sum_k Q(k,i). \quad (8)$$

This is the modified Richardson-Lucy (RL) equation. It shares a similar form with the original RL equation (Richardson, 1972; Lucy, 1974) but with the background taken into consideration properly and is adapted to the reconstruction task of the modified modulation equation. While the original RL equation can be considered as achieving a maximum likelihood solution of the modulation equation for Poisson noise dominated data, satisfying nonnegative constraint, the modified RL equation reaches that with a stricter background constraint, thus giving a better estimation of the object. Actually, Knödlseder et al. (1999; 2007) have developed such kind of modified RL equation. Our work however demonstrates that it can be also adapted to the flux reconstructions of variable sources, if one replaces the normal response matrix with the modified response matrix. From Eq. (8) one could derive the quiescence flux and bursting flux of time-varying object simultaneously. By the way, one may find that the modified RL equation with normal response matrix is more or less equivalent to the simplest implementation of the original DD method as they both use the background constraint.

### 2.3. The improved DD method

It is obvious from Eq. (8) that in order to solve the modified modulation equation, two variables are needed: the background and the modified response matrix. In the case of having no *priori* knowledge on the background, we estimate it from the observational data via the SNIP method (Ryan et al., 1988; Morháč et al., 1997), popularly used in nuclear physics. The key point to build the modified response matrix is to know when the bursts occur, which can be estimated with the original DD method and is illustrated in what follows. Since as we know that the steady sources (including long-term variable sources that can be regarded approximately stable in an individual scanning observation) can be recovered properly with the original DD method and removed from the observational data, any additional short-term drastic variation (like bursts from a source) will be visible from the residual of the scanning light curve. Their occurrences can be located from the residual light curve by an automatic peak-searching technique.

Thus, the improved DD method will go through the following steps:

(1) Estimate the background with the SNIP method.
(2) Reconstruct the sky image with the original DD method or the modified RL equation with normal response matrix.
(3) Remove the steady sources from the light curve and search for additional bursts or structures with short time variabilities using an automatic peak-searching technique. This technique is based on the PEAKFINDS function of MATLAB software, in which the widths and heights of the peaks are important parameters for excluding pseudo-peaks caused by statistical fluctuations.
(4) Build the modified response matrix. Two kinds of circumstances are considered: (a) For a known variable source, the response matrix elements can be determined through the source's position relative to the pointing of the telescope (Nang et al., 2020). Then only the elements corresponding to the bursting time derived in step (3) are chosen to be included in the matrix and the others are replaced with zero. (b) If there exists an unknown variable source in the field, a blind search for the best position will be carried out among the grids that are centered on the preliminary position of the variable source estimated in step (2). Each grid represents a trial and the construction of the modified response matrix for each trial is the same as that described in (a).
(5) Reconstruct the observed data with Eq. (8) (the modified RL equation with modified response matrix). A parameter $E$ which is the sum of the squares of the deviations normalized by the variances (Lu et al., 1996) gives a quantitative description of the convergence of the iteration. $E = \sum_{k=1}^{M} \frac{(d(k)T-d'(k)T)^2}{d'(k)T}$, where $d(k)$ is the observed count rate, $d'(k)$ is the derived predicted count rate and $T$ is the observational time at every bin. The minimum of the parameter $E$ at each iterative step determines the stopping criterion of the iteration. The parameter $E$ could also be used for model comparison. For case (b) described in step (4), repeat the reconstruction for each trial and the minimum of the parameter $E$ of all the trials determines the best position of the variable source.
(6) Use Bootstrap technique to estimate the statistical errors and confidence levels of the parameters: generate a number of Bootstrap samples (i.e. light curves) from the observed light curves by *random resampling with replacement* (Efron, 1979; Simpson and Mayer-Hasswander, 1986), then analyze each Bootstrap sample following the preceding steps (1-5), calculate the statistics of interest (like positions and intensities) for each Bootstrap sample, and eventually determine the confidence intervals from the frequency distribution of the parameters obtained from all the Bootstrap samples.

## 3. Applications and results

The MC simulated data and real data of *Insight-HXMT*/LE are used to test the performance and verify the feasibility of the improved DD method.

### 3.1. The LE payload and the observational strategy

The LE payload consists of three detector boxes and each box contains 32 CCD236 detectors. The sensitive area of one CCD236 detector is about 4 $cm^2$. For each detector box, collimators above the CCD236 detectors define four kinds of FoVs. Twenty CCD236 detectors have small FoVs with $1^\circ.6 \times 6^\circ$. Six have large FoVs with $4^\circ \times 6^\circ$. Two have blind FoVs. And four have a very large FoV with about $(50^\circ - 60^\circ) \times (2^\circ - 6^\circ)$ (Chen et al., 2019). Only small FoV detectors are investigated in this work because larger FoV detectors are most likely illuminated by the bright Earth (Chen et al., 2018; Huang et al., 2018). As the FoVs of one box share the same orientation and have a cross angle of 60° with that of the other two boxes, data recorded by one box can be combined together to generate a light curve and therefore three light curves corresponding to the three boxes are derived for later reconstruction analysis. The PSF model of LE, which reflects the geometrical effects of the collimators, i.e. the detection efficiency of the telescope to a point source in its FoV, is used to build the response matrix.

The survey of the Galactic plane is accomplished patch by patch (Fig. 2), each with a size of $(14^\circ - 20^\circ) \times (14^\circ - 20^\circ)$. Overlapped patches in the Galactic center ensure more exposure time on the Galactic bulge region. The scan of one patch is carried out with the small area scan mode (Fig. 3) and takes 2 hours to 5 days depending on combinations of the different scan parameters: The radius of the scanned region ranges between $7^\circ - 10^\circ$; the scanning speed along each scanning line can be chosen as $0^\circ.01$/s, $0^\circ.03$/s or $0^\circ.06$/s; the distance between adjacent scanning lines is between $0^\circ.1 - 1^\circ$. A combination of scanning radius of 7°,

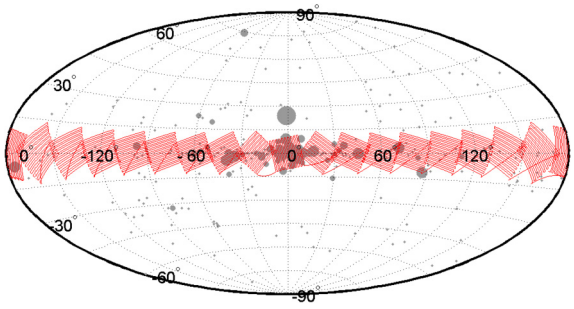


**Fig. 2.** Scanning strategy of the Galactic plane.

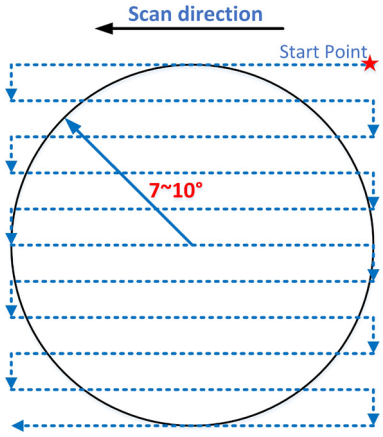


**Fig. 3.** Illustration of how a small sky area is scanned with *Insight-HXMT*.

**Table 1**
Comparison between the input and reconstructed flux.

| Source | | Input flux (photons/s/cm$^2$) | Restored flux (photons/s/cm$^2$) | |
|---|---|---|---|---|
| | | | Original DD | Improved DD |
| source 1 | Quiescence | 0.15 | 0.30 ± 0.013 | 0.17 ± 0.019 |
| | Burst1 | 0.5 | | 0.48 ± 0.039 |
| | Burst2 | 0.3375 | | 0.36 ± 0.078 |
| | Burst3 | 0.3375 | | 0.30 ± 0.075 |
| | Burst4 | 0.25 | | 0.27 ± 0.049 |
| source 2 | | 0.11 | 0 ± 0.015 | 0.08 ± 0.021 |
| source 3 | | 0.21 | 0.26 ± 0.013 | 0.24 ± 0.015 |
| source 4 | | 0.57 | 0.58 ± 0.004 | 0.58 ± 0.010 |
| source 5 | | 1.4 | 1.42 ± 0.022 | 1.42 ± 0.039 |
| source 6 | | 1.92 | 1.89 ± 0.005 | 1.89 ± 0.017 |

scanning speed of 0°.06/s and the scanning interval of 0°.4 was adopted since March 30th in 2019 observation.

### 3.2. Application to simulated data

We simulate two kinds of variable sources with different activity durations to test the applicability of the improved DD method: Type-II burster (with variation time scale much shorter than the scanning time of one patch of the Galactic plane); SFXT (with variation time scale nearly equal to the scanning time).

#### 3.2.1. Type-II burster

We simulate an LE scanning observation of a Type-II burster undergoing four bursts in a crowded region. The flux of its persistent emission is set to 0.15 photons/s/cm$^2$ and those of the bursts are set to 0.5, 0.3375, 0.3375, 0.25 photons/s/cm$^2$ with durations of 12 s, 12 s, 8 s, 12 s, respectively. The fluxes of other five steady point sources are listed in Table 1. The PSF model of the small FoV of the three detector boxes of LE is used here to build the response matrix. The observations are simulated by using the same parameters as for the real *Insight-HXMT* Galactic plane survey. With such a scanning mode, a configured response matrix, a faked object, and a uniform background of 4 cts/s for all the small FoV detectors in one box which is consistent with the average in-orbit background of LE, we derive the simulated light curves of LE in units of counts per second (see Fig. 4).

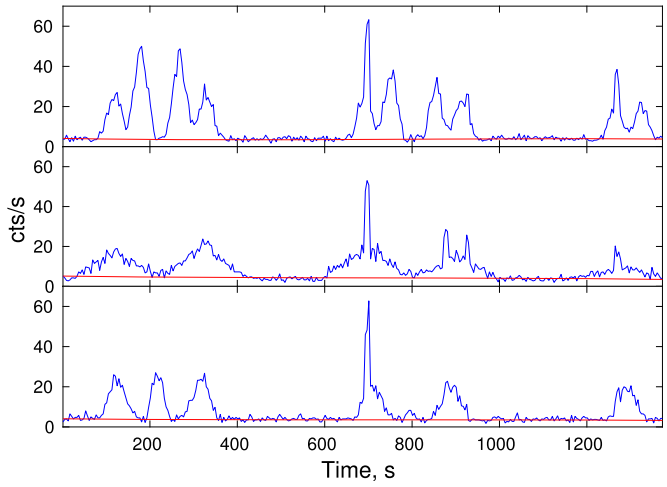


**Fig. 4.** Simulated light curves (blue lines) for the three detector boxes of LE (hereinafter is the same) and the estimated background by the SNIP method (red lines). (For interpretation of the colors in the figure(s), the reader is referred to the web version of this article.)

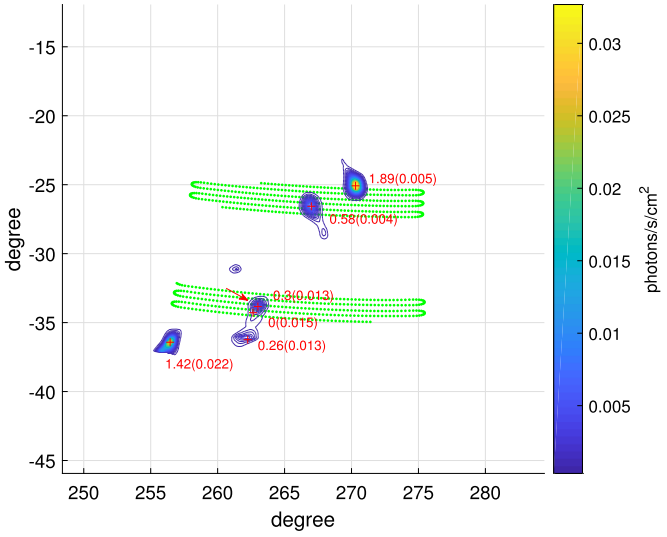


**Fig. 5.** Blue contours show the reconstructed image with the original DD method. The red crosses represent the positions of the reconstructed point sources labeled with the restored flux and flux error. The red arrow indicates the Type-II burster. The green dotted lines illustrate the scanning paths of the satellite. The gaps are due to non-observing intervals during Earth occultation and during passages through the South Atlantic Anomaly region.

We reconstruct the object from the faked light curve using both the original DD method and the improved DD method as described in section 2.3. Fig. 5–Fig. 8 are the comparison of the reconstructed results of the two methods. The original DD map (Fig. 5) shows that discrete steady sources can be well reconstructed with restored fluxes almost equal to the input ones. However, the variable source (i.e. the Type-II burster) is poorly reconstructed, with all bursts left in the residual light curves (Fig. 6) and an overestimated quiescence flux. Besides, the reconstruction of the nearby source (0°.57 away from the Type-II burster) is affected. These problems can be solved by the improved DD method. Both the qui-

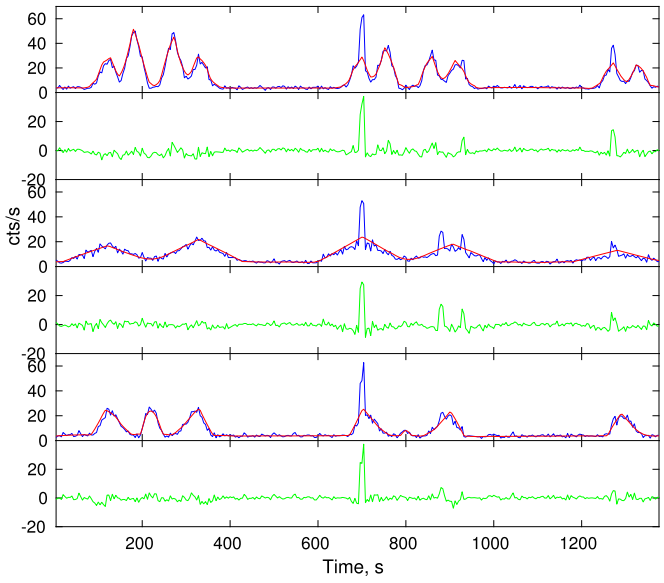


**Fig. 6.** Comparison between the predicted light curves derived with the original DD method (red lines) and the observed ones (blue lines). Green lines shows the residuals between them.

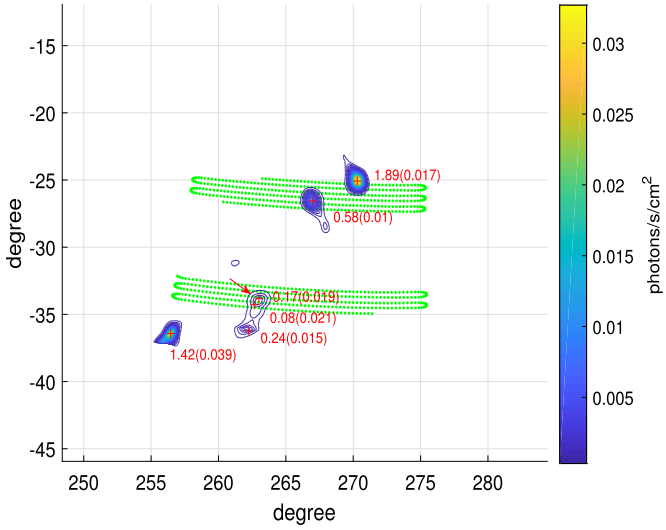


**Fig. 7.** The same as Fig. 5 but with the improved DD method.

escence flux (Fig. 7) and the burst flux are well reconstructed and a good agreement between the input and the predicted light curves has been achieved (Fig. 8). A quantitative comparison between the input and restored flux, as shown in Table 1, demonstrates the capability of the improved DD method for handling the reconstruction of the very short term variation.

### 3.2.2. SFXT

A SFXT can produce very bright X-ray flares of short duration, lasting from a few minutes to a few hours, but no detectable quiescence emission. An interesting flare was reported from the IGR J16479–4514 (Sguera et al., 2005), with a very rapid rise lasting $\sim 5$ minutes followed by a slow exponential decay lasting $\sim 25$ minutes, similar to a thermonuclear Type-I X-ray burst. Thus an LE observation of a region with such a SFXT (Fig. 9) and other two steady point sources is simulated. The input parameters used in the simulation are listed in Table 2 and Table 3. Other configurations of the simulation are the same as that described in

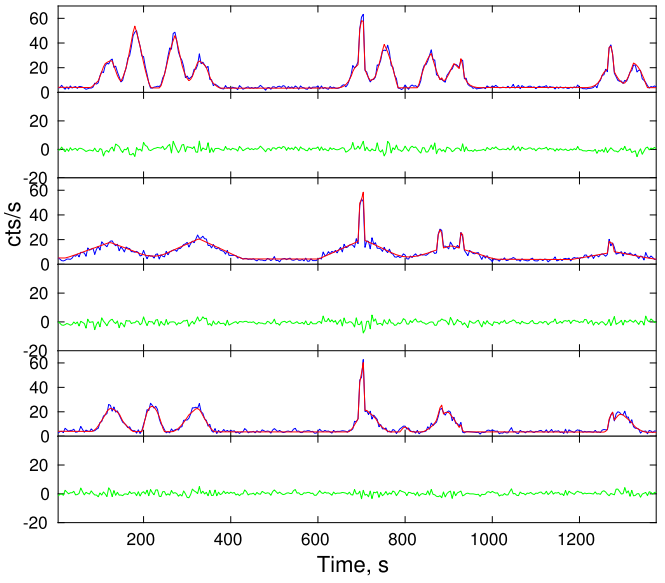


**Fig. 8.** The same as Fig. 6 but with the improved DD method.

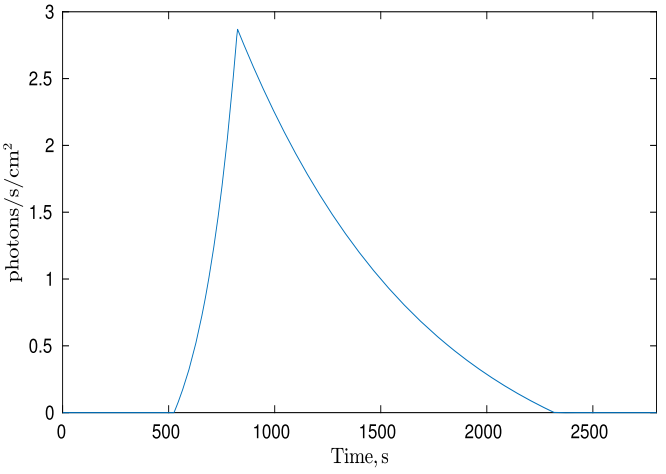


**Fig. 9.** The input light curves of a SFXT.

**Table 2**
Comparison between the input and reconstructed results.

| Source | | Input | Restored results | |
|---|---|---|---|---|
| | | | Original DD | Improved DD |
| SFXT | Ra(deg) | 153.11 | 153.06 ± 0.049 | 153.12 ± 0.028 |
| | Dec(deg) | -54.83 | -54.44 ± 0.010 | -54.83 ± 0.018 |
| | flux[a] | a light curve | 1.04 ± 0.020 | a light curve |
| source 2 | flux[a] | 1 | 0.95 ± 0.012 | 0.95+-0.011 |
| source 3 | flux[a] | 1.5 | 1.27 ± 0.021 | 1.48 ± 0.018 |

[a] in units of photons/s/cm$^2$.

section 3.2.1. Finally, we obtain the simulated light curves of LE in units of counts per second (see Fig. 10).

Fig. 11 shows the reconstructed image by the original DD method. The SFXT has been reconstructed as a steady source: the flux during each flare is underestimated but with spurious flux before and after each flare (Fig. 12). The reconstruction of the nearby source (1°.67 away from the SFXT) is affected because its peaks in the light curves overlap that of the SFXT. However the reconstructed position of the SFXT is marginally correct (see Table 2), which is a useful hint for the improved DD method when no *priori* information of the position is known for a new SFXT. Then a search

**Table 3**
Comparison between the input and reconstructed parameters of the SFXT.

| Parameters | Input | Restored results with improved DD |
|---|---|---|
| Peak position (min) | 13.75 | 13.74 ± 0.157 |
| Time scale of the rising state (min) | 3 | 3.16 ± 0.542 |
| Time scale of the decay state (min) | 15 | 15.43 ± 1.005 |
| Peak value (photons/s/cm$^2$) | 2.87 | 2.84 ± 0.152 |

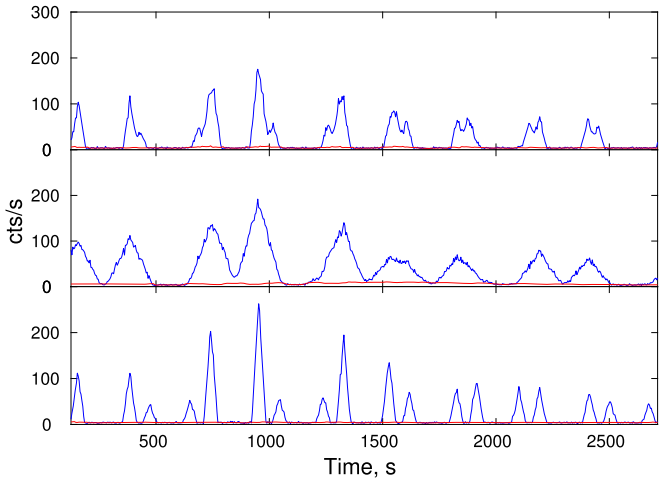


**Fig. 10.** Simulated light curves (blue lines) and the estimated background by SNIP method (red lines).

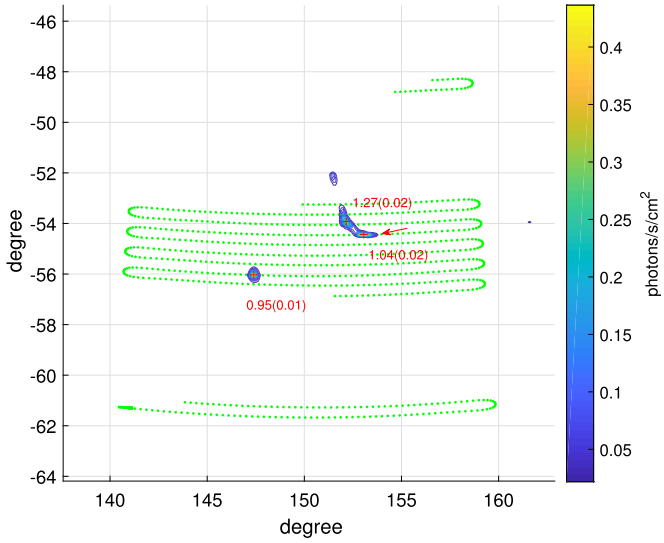


**Fig. 11.** Blue contours show the reconstructed image with the original DD method. The red crosses represent the positions of the reconstructed point sources labeled with the restored flux and flux error. The red arrow indicates the SFXT. The green dotted lines illustrate the scanning paths of the satellite. The gaps are due to non-observing intervals during Earth occultation and during passages through the South Atlantic Anomaly region.

around the position is carried out with the improved DD method to find the best position as described in section 2.3. This results in a much more precise position (Table 2), as well as a variable light curve of the SFXT (red squares in Fig. 15) and more accurate flux of the nearby source. Hence the predicted light curves match the input ones quite well (Fig. 14). Note that no detection of the SFXT is left on restored image (Fig. 13) because of no quiescence emission from the SFXT. Finally, we fit the restored light curve of the SFXT to a model with a fast rising followed by a slow decay (green

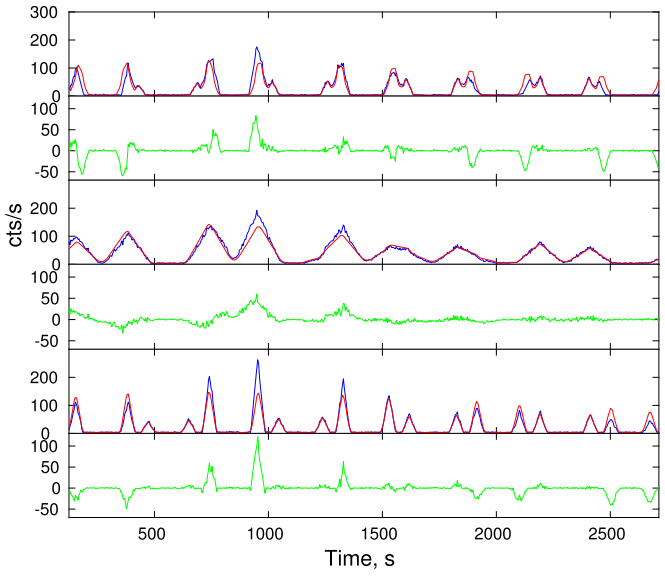


**Fig. 12.** Comparison between the predicted light curves derived with the original DD method (red lines) and the observed ones (blue lines). Green lines shows the residuals between them.

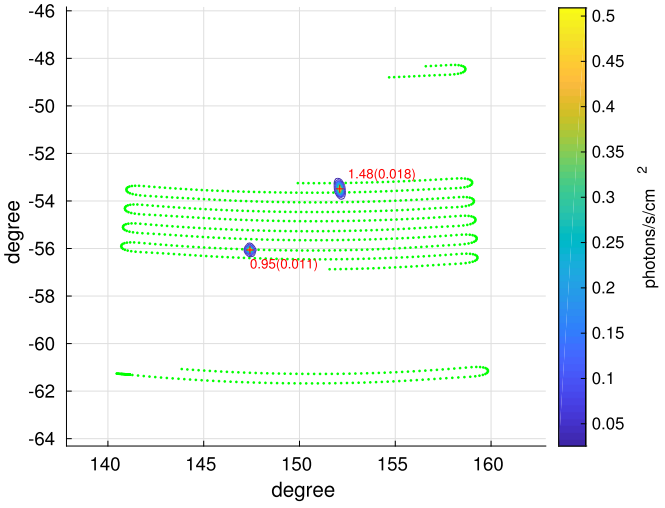


**Fig. 13.** The same as Fig. 11 but with the improved DD method.

line in Fig. 15) and derive the characteristic parameters which are consistent with the input ones (Table 3). Note that the first two clusters of the residual (black squares in Fig. 15) are slightly uptilted because of the coupling of the flux between the SFXT and the nearby source due to their overlapping peaks.

### 3.3. *Application to real* Insight-HXMT/*LE data*

*Insight-HXMT* carries out the Galactic plane survey at a frequency of once every a few days since its launch in 2017. After being received, the observational data are analyzed by the offline pipeline automatically. Such a quick look can result in some early results from *Insight-HXMT* observation, e.g. the detection of a series of fast short bursts from LE during 2019 April 7th (MJD 58580) to 14th (MJD 58587) from the Rapid Burster MXB 1730–335. Part of the burst data in the observation ID P0211007023 (MJD 58581) with good time window are used in this work.

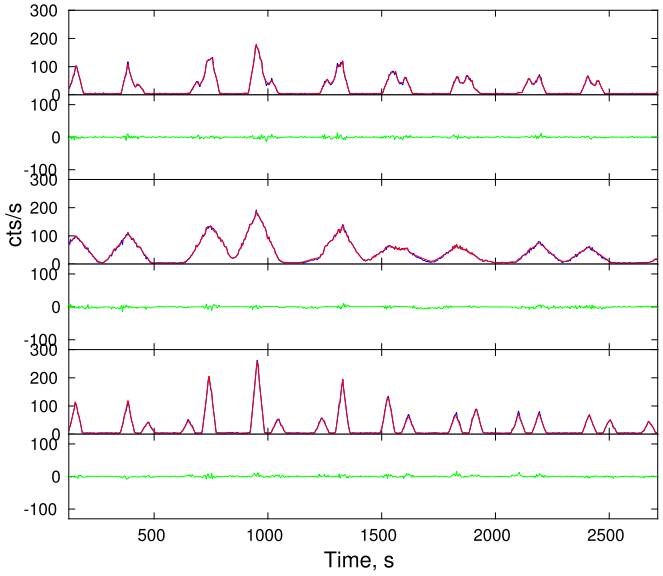


**Fig. 14.** The same as Fig. 12 but with the improved DD method.

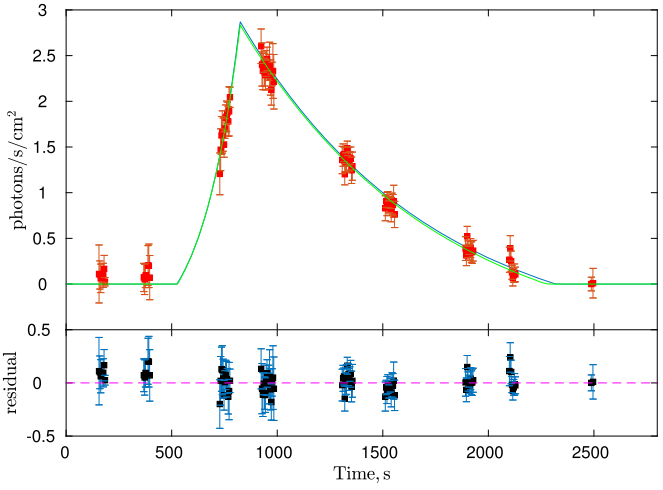


**Fig. 15.** Fitting the restored flux of the SFXT (red square) to a model with a rapid rise and a slow exponential decay (green line). The lower panel shows the fitting residual. The input light curve (blue line in the upper panel) is given for comparison.

### 3.3.1. Data reduction

Before performing the improved DD analysis, the observational data have to be filtered in order to have better data quality. We use the following standard filtering criteria (Zhao et al., 2016) to LE data selection: (1) elevation angle (ELV) larger than 10°, (2) elevation angle from the day Earth's limb (DYE_ELV) larger than 30°, (3) the geometric cutoff rigidity (COR) larger than 6, (4) time before and after South Atlantic Anomaly (SAA) region (T_SAA and TN_SAA) larger than 50 s, and (5) the cumulated count rate of all trigger events not lower than 3000 cts/s. After filtering, we select photons in the energy range $1-6.1$ keV recorded by the small FoV detectors of LE to generate the light curves. The detectors with large FoV of LE are discarded due to that they are most likely illuminated by the bright Earth. The blue lines in Fig. 16 show the light curves with bin-size of 4 s, detected by the small FoV detectors of the three boxes of LE. The SNIP method is then applied to extract the background (see red lines in Fig. 16) from these light curves.

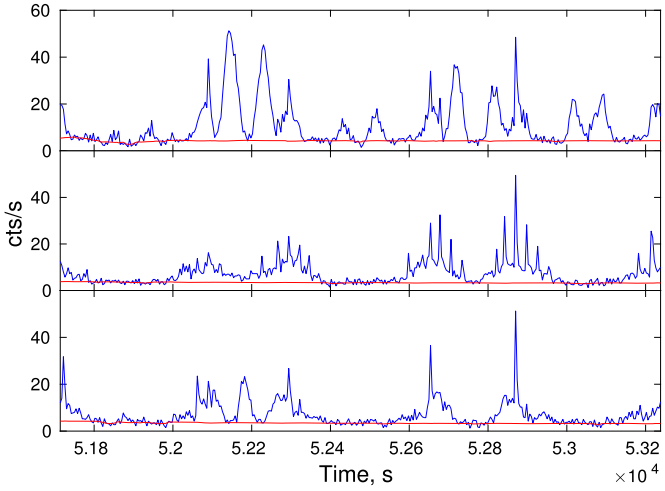


**Fig. 16.** *Insight-HXMT*/LE $1-6.1$ keV light curves (blue lines) and the estimated background by SNIP method (red lines). (The time has been subtracted by 229300000 s and the date of the zero time is 2012-01-01T00:00:00. Hereinafter is the same.)

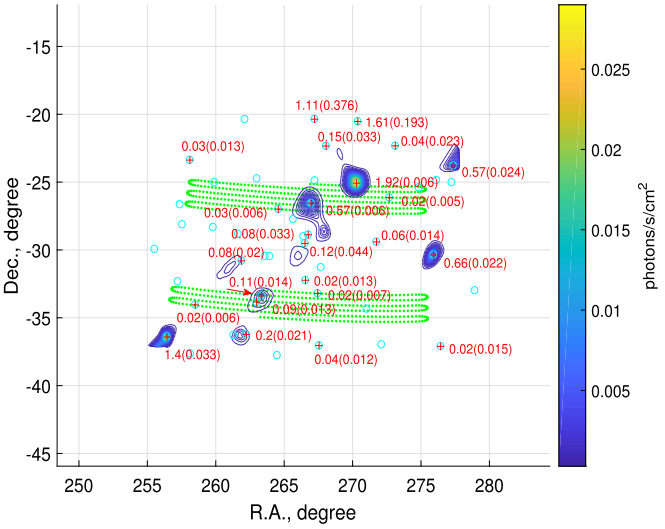


**Fig. 17.** Blue contours show the reconstructed image with the original DD method. The red crosses represent the positions of reconstructed point sources labeled with the restored flux and flux error, while cyan circles represent positions from MAXI source catalog. The red arrow indicates the Rapid Burster MXB 1730–335. The green dotted lines illustrate the scanning paths of the satellite. The gaps are due to non-observing intervals during Earth occultation and during passages through the South Atlantic Anomaly region.

### 3.3.2. Reconstruction and comparison

We first reconstruct the observed light curves with the original DD method. As shown in Fig. 18, the light curves obtained with the original DD analysis are sometimes not consistent with the observational data. It confirms again the experience learned from the MC simulation that the original DD method cannot reconstruct the fast and short bursts that reside in the observational data, simply because the source flux no longer remains stable. However, as indicated in Fig. 18, the residuals in the observational light curves after the subtraction of the restored light curves, provide us information on when the bursts occur and how long they last, by taking an automatic peak-searching technique. Twenty bursts with duration of $\sim 10$ s each recorded in an observational segment lasting for 620 s mean that we observed a sequence of bursts with a rate of $\sim 2$ events per minute from the Rapid Burster MXB 1730–335. Then we analyze the observational data with the improved DD method

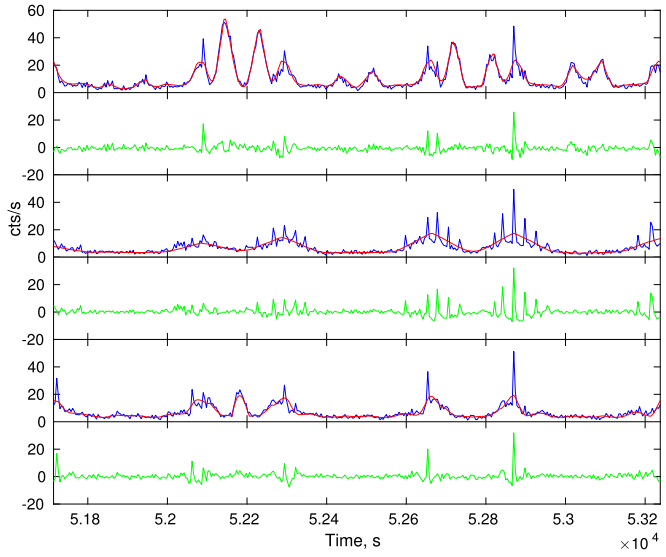


**Fig. 18.** Comparison between the predicted light curves derived with the normal DD method (red lines) and the observed ones (blue lines). Green lines shows the residuals between them.

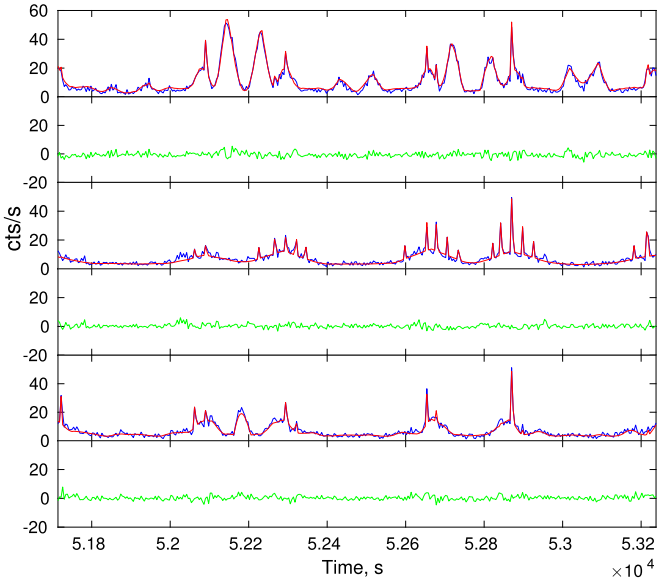


**Fig. 20.** The same as Fig. 18 but with the improved DD method.

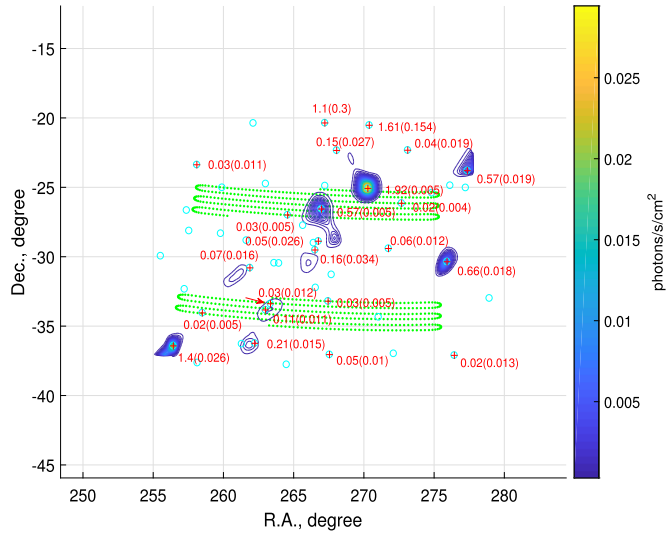


**Fig. 19.** The same as Fig. 17 but with the improved DD method.

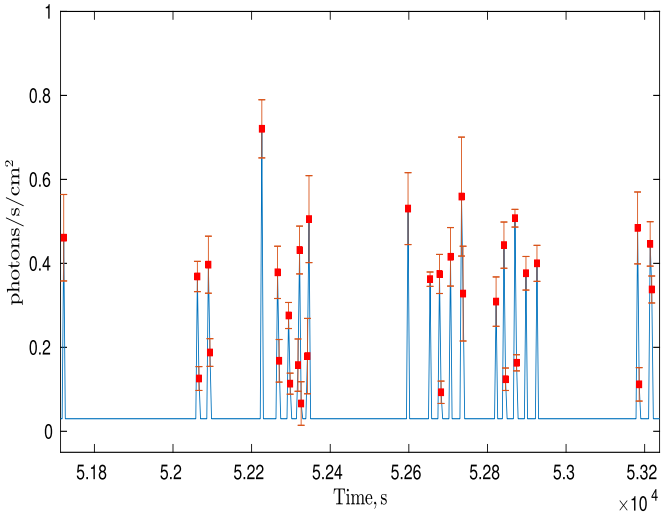


**Fig. 21.** The monitoring light curve of MXB 1730–335 by *Insight-HXMT*/LE. The baseline represents the flux of quiescence while red squares mark the flux of the bursts.

and show the reconstructed sky image in Fig. 19. Compared with the reconstructed image with the original DD method (Fig. 17), not only a bunch of stable point sources but also the Rapid Burster and nearby sources are properly reconstructed. A nice match between the predicted light curves and the observed ones (Fig. 20) is obvious, which indicates the capability of the improved DD method in processing the variable sources. Finally, we show the resulted light curve of MXB 1730–335 with timescale of 4 s in Fig. 21 and calculate the fluence of each burst and its waiting time to next one. A plot of the correlation between them is shown in Fig. 22, where one sees clear positive correlation between the burst fluence and its waiting time. This is consistent with the previous report for a relaxation-oscillator behavior observed in the Rapid Burster with other X-ray telescopes (Bagnoli et al., 2015).

## 4. Conclusion and discussion

In this paper, we develop a modified RL equation and propose an improved DD method, which can reconstruct the fluxes of variable objects from the scan observation data. The applications of this method to simulated and real *Insight-HXMT* data demonstrate its effectiveness. More precise location of the variable source is obtained, as well as the quiescence and bursting fluxes, thus making more precise flux monitoring possible. The new method takes effect mainly for two principles: the modified RL equation could be seen as containing another kind of background constraint, which plays an important role in the development of effective and efficient algorithms for that it could provide for a stable and unique solution; the key point of the improved DD method is the reconstruction of the modified response matrix, in which the variability of the source is properly handled.

The Rapid Burster MXB 1730–335 is a well-known low mass X-ray binary (LMXRB) featured with both Type-I and Type-II burst. Our results obtained with the improved DD method shows that it is in a state with frequent Type-II bursts in a manner of the well-known relaxation oscillation. More precisely, MXB 1730–335 appears to be in the Phase II, Mode II of the classification by Marshall et al. (1979): all the events occur almost regularly (at a time distance of about 30 s) and have short time durations (about 10 s).

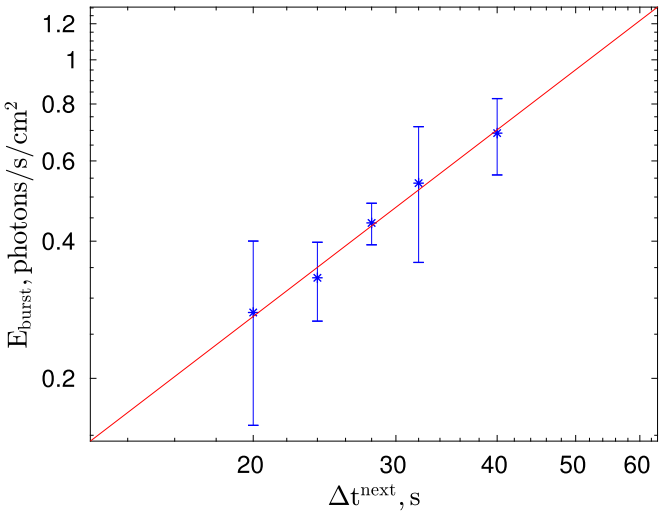


**Fig. 22.** Burst fluence as a function of the waiting time to the next burst. The least-squares fit to the data is shown with a red line.

SFXTs are a kind of fast and short X-ray transients. Their unusual short and luminous outbursts make them particularly interesting. But as they occur at serendipitous positions sporadically with very short duration, they are difficult to detect and supposed to be best detected and discovered by instruments having a sufficiently wide field of view and high sensitivity. *Insight-HXMT*/LE may serves as a useful instrument for detecting SFXTs, thanks to its relatively high sensitivity and wide field of view as well as the Core Program of the mission to survey the Galactic plane. With the aid of the improved DD method, ongoing observations of the Galactic plane with *Insight-HXMT* may yield further detections of such sources.

## Acknowledgments

This work made use of the data from the *Insight-HXMT* mission, a project funded by China National Space Administration (CNSA) and the Chinese Academy of Sciences (CAS). The authors thank supports from the National Program on Key Research and Development Project (Grant No. 2016YFA0400802) and the National Natural Science Foundation of China under Grants No. U1838202, U1838201 and 11703028.

## References

Bagnoli, T., in't Zand, J.J.M., D'Angelo, C.R., et al., 2015. Mon. Not. R. Astron. Soc. 449, 268.
Cao, X.-L., Jiang, W.-C., Meng, B., et al., 2019. Sci. China, Phys. Mech. Astron. https://doi.org/10.1007/s11433-019-1506-1, in press. arXiv:1910.04451.
Chen, Y., Li, T.-P., Wu, M., 1997. In: Proc. ADASSVI. In: ASP Conf. Ser., vol. 125, p. 178.
Chen, Y., Cui, W.-W., Li, W., et al., 2019. Sci. China, Phys. Mech. Astron. in press. arXiv:1910.08319. https://doi.org/10.1007/s11433-019-1469-5.
Chen, Y.-P., Zhang, S., Qu, J.-L., et al., 2018. Astrophys. J. Lett. 864, 5.
Efron, B., 1979. Rietz lecture. Ann. Stat. 7, 1.
Feng, H., Chen, Y., Zhang, S.-N., et al., 2003. Astron. Astrophys. 402, 1151.
Gull, S.F., Daniell, G.J., 1978. Nature 272, 686.
Huang, Y., Qu, J.-L., Zhang, S., et al., 2018. Astrophys. J. 866, 122.
Knödlseder, J., Dixon, D., Bennett, K., et al., 1999. Astron. Astrophys. 345, 813.
Knödlseder, J., Weidenspointner, G., Jean, P., et al., 2007. ESA SP 622, 13.
Li, T.-P., 2003. Imaging in Hard X-ray Astronomy. In: Li, X.D., Trimble, V., Wang, Z.R. (Eds.), Proceedings of the 214th Symposium of the International Astronomical Union. Astronomical Society of the Pacific, China.
Li, T.-P., Wu, M., 1993. Astrophys. Space Sci. 206, 91. https://doi.org/10.1007/BF00658385.
Li, T.-P., Wu, M., 1994. Astrophys. Space Sci. 215, 213. https://doi.org/10.1007/BF00660079.
Liu, C.-Z., Zhang, Y.-F., Li, X.-F., et al., 2019. Sci. China-Phys. Mech. Astron. https://doi.org/10.1007/s11433-019-1486-x, in press. arXiv:1910.04955.
Lu, F.-J., Li, T.-P., Sun, X.-J., et al., 1995. In: Shellard, Nguyen (Eds.), Proceedings of CHEP'95, p. 848.
Lu, F.-J., Li, T.-P., Sun, X.-J., et al., 1996. Astron. Astrophys. Suppl. Ser. 115, 395.
Lucy, L.B., 1974. Astron. J. 79, 745.
Marshall, H.L., Hoffman, J.A., Doty, J., et al., 1979. Astrophys. J. 227, 555.
Morháč, M., Kliman, J., Matoušek, V., et al., 1997. Nucl. Instrum. Methods Phys. Res., Sect. A 401, 113.
Nang, Y., Liao, J.-Y., Sai, N., et al., 2020. J. High Energy Astrophys. 25, 39. https://doi.org/10.1016/j.jheap.2020.01.002.
Paizis, A., Sidoli, L., 2014. Mon. Not. R. Astron. Soc. 439, 3439.
Richardson, W.H., 1972. J. Opt. Soc. Am. 62, 55.
Ryan, C., Clayton, E., Griffin, W., et al., 1988. Nucl. Instrum. Methods Phys. Res., Sect. B 34, 396.
Sguera, V., Barlow, E.J., Bird, A.J., et al., 2005. Astron. Astrophys. 444, 221.
Shen, Z.-J., Zhou, J.-F., 2008. Chin. J. Astron. Astrophys. 8, 343.
Simpson, G., Mayer-Hasswander, H., 1986. Astron. Astrophys. 162, 340.
Song, L.-M., Li, T.-P., Cui, W., 1999. Acta Astrophys. Sin. 19, 27.
Starck, J.L., Murtagh, F., 2006. Astronomical Image and Data Analysis, first edition. Springer-Verlag, Berlin, p. 61.
Zhang, S., Li, T.-P., Wu, M., 1998. Astron. Astrophys. 340, 62.
Zhang, S.-N., Li, T.-P., Lu, F.-J., et al., 2019. Sci. China, Phys. Mech. Astron. in press. arXiv:1910.09613. https://doi.org/10.1007/s11433-019-1432-6.
Zhao, H.-S., Li, C.-K., Li, X.-B., et al., 2016. Chin. J. Space Sci. 36, 938.